Eccentricity and inclination damping of terrestrial embryos in the protoplanetary gas disc

John Gillan, Michiel Lambrechts, Sebastian Lorek

1 Abstract

In this work we simulate many Mars mass bodies interacting with each other and with the gas-disc in the early solar system. Interactions between planets stir them up and increase both their eccentricity and inclination. They feel tidal forces from the gas disc which result in damping of eccentricity and inclination, and inward migration. We compare two different damping prescriptions from the literature. In almost all cases eccentricity and inclination are damped below H/r. Collisional growth strengthens damping.

2 Introduction

Planets are found at a range of distances from their host star. They are thought to migrate after their formation, as a result of their interaction with the surrounding gas in the protoplanetary disc in the early stages of the systems formation. Early interactions with other planets in the same system should excite the orbits of planets in systems with multiple planets, increasing their eccentricity and inclination. However observations show that planets generally have low eccentricity and inclination, particularly noticeable in our own solar system, where most of the planets have almost circular orbits around the sun. An explanation for this evolution from dynamically hot to dynamically cold is the gravitational interaction between the planet and the surrounding gas. As a planet orbits its host star in a protoplanetary disc, the gas in the disc will have its own orbital speed depending on its distance from the star. Gas closer to the star will have a higher orbital speed while gas farther away from the star will have a lower orbital speed. A planet with a high eccentricity will change its distance from the star during its orbit, and so will pass through regions of gas with different orbital

velocities to the planet. This will produce a torque on the planet, lowering its eccentricity. If the planet is on a circular orbit, these interactions with the gas will lower its semi-major axis. This is known as 'Type 1 migration'. Ideally, to examine how this process occurs, combinations of hydrodynamical and N-body simulations of multiple planets in a protoplanetary disc are required. However, this becomes extremely computationally expensive when carried out over the timescales needed. To overcome this problem, N-body codes are used with added forces for the eccentricity, semi-major axis, and momentum damping, which represent the effects of the gas disc on the planet.

There have been many attempts at creating prescriptions for N-body codes that accurately represent the migration and eccentricity damping of planetary embryos in the disc gas (Ida et al. 2020 [1]; Cresswell & Nelson 2008 [2]). Each prescription is based on a damping timescale, t_{wave}, given by [3]:

$$t_{wave} = \frac{M_{star}}{M_p} \frac{M_{star}}{\Sigma a^2} h^4 \Omega^{-1} \tag{1}$$

where a is the semi-major axis of the planet, Σ is the surface density of the gas at that distance from the star, Ω is the Keplerian frequency, and $h = H/r = 0.05$ is the scale height of the disc. t_{wave} is then built upon to create the damping timescales for the different components of the orbit. Here we compare the eccentricity and semi-major axis damping timescales calculated from the prescriptions from Ida et al. 2020 [1] and Cresswell & Nelson 2008 [2].

3 Damping timescale prescriptions

Cresswell & Nelson 2008 derive the expression for the eccentricity damping timescale as:

$$t_e = \frac{t_{wave}}{0.780}(1 - 0.14\hat{e}^2 + 0.06\hat{e}^3 + 0.18\hat{e}\hat{i}^2) \tag{2}$$

where $\hat{e} = e/h$ and $\hat{i} = i/h$ with $h = H/r$. They give the expression for the momentum damping timescale as:

$$t_m = \frac{2 \times t_{wave}}{h^2(2.7 + 1.1p)} \frac{1 + (\frac{\hat{e}}{2.25})^{1/2} + (\frac{\hat{e}}{2.84})^6}{1 - (\frac{\hat{e}}{2.02})^4} \tag{3}$$

where p is calculated from how the surface density of the disc changes as a function of radius:

$p = -d\ln\Sigma/d\ln r$. The expression for the semi-major axis damping timescale is calculated from both the eccentricity and momentum damping timescales:

$$t_a = \left(\frac{2}{t_m} + \frac{2e^2}{t_e}\right)^{-1} \tag{4}$$

Their inclination damping timescale is:

$$t_i = \frac{t_{wave}}{0.780}(1 - 0.30\hat{i}^2 + 0.24\hat{i}^3 + 0.14\hat{i}\hat{e}^2) \tag{5}$$

Ida et al 2020 attempted to find simpler and more accurate prescriptions. Their simplified expression for the eccentricity damping timescale is:

$$t_e = \frac{t_{wave}}{0.780} \times \left[1 + \frac{1}{15}(\hat{e}^2 + \hat{i}^2)^{3/2}\right] \tag{6}$$

They calculate the semi-major axis damping timescale as:

$$t_a = \frac{t_{wave}}{C_t h^2}\left(1 + \frac{C_T}{C_M}(\hat{e}^2 + \hat{i}^2)^{1/2}\right) \tag{7}$$

where they use $C_T = (2.73 + 1.08p + 0.87q)$ and $C_M = 6(2p - q + 2)$. q is found with $q = -d\ln T/d\ln r$, and p is found with $p = -d\ln\Sigma/d\ln r$. Their inclination damping timescale is:

$$t_i = \frac{t_{wave}}{0.544} \times \left[1 + \frac{1}{21.5}(\hat{e}^2 + \hat{i}^2)^{3/2}\right] \tag{8}$$

The momentum damping timescale is found using the other three timescales:

$$t_m = \left(\frac{1}{2t_a} - \frac{e^2}{t_e} - \frac{i^2}{t_i}\right)^{-1} \tag{9}$$

We compared the two prescriptions given above. The different damping timescale formulae were first plotted for a system with one planet orbiting a sun-like star. t_{wave} was found by using a solar mass star and a 10 earth mass planet at 1 AU from the star. Cresswell & Nelson set the surface density of the disc to $\Sigma = 1700(a/AU)^{-1/2}$, $p = 0.5$, $q = 1$, $C_T = 4.14$ and

$C_M = 12$. Ida et al set the surface density of the disc to $\Sigma = 1700(a/AU)^{-1}$, $p = 1$, $q = 0.5$, $C_T = 4.25$ and $C_M = 21$. The equations were plotted as a function of time in years. The prescriptions for eccentricity and semi-major axis damping with an initial inclination of zero are compared in Figure (1). For the eccentricity damping timescale this shows the time to circularization. Figure (2) shows the damping timescales for inclination and semi-major axis with zero initial eccentricity.

The eccentricity was also examined by selecting a particular initial eccentricity and then integrating forward in time-steps of 0.01 of a year using Euler integration. At each time-step the new eccentricity was used to calculate the new t_e. This gives a plot of how the eccentricity will change over time from an initial value. This was repeated for several different initial eccentricities. The results from the damping prescriptions from Cresswell & Nelson are shown in Figure (3).

4 Equations of motion

Both the Ida prescription and the Cresswell & Nelson prescription provide force equations that can be used in N-body code to govern the motion of planets in a protoplanetary disc. Cresswell & Nelson define the accelerations experienced by the protoplanets due to the disc as:

$$\frac{\mathrm{d}\mathbf{v}}{\mathrm{d}t} = -\frac{\mathbf{v}}{t_m} - 2\frac{(\mathbf{v}\cdot\mathbf{r})\mathbf{r}}{r^2 t_e} - \frac{v_z}{t_i}\mathbf{k} \tag{10}$$

where $\mathbf{k}$ is the unit vector in the z direction, and v_k is the velocity in the z direction. We examined this prescription using a custom built 4th order Runge-Kutta integrator which takes in a force equation and integrates it forward in time by a set time-step which does not change. For the Cresswell & Nelson prescription we placed a 10 earth mass planet at 1 AU from a 1 solar mass star. The inclination was kept at zero. This meant that the last term in equation (10) was equal to zero. The acceleration according to the Cresswell & Nelson prescription is calculated from the velocity vector and the position vector of the planet at every time-step. This acceleration was added to the acceleration due to the stars gravity at each step in the integrator. This is a simpler prescription than that recommended by Ida et al. A time-step of 0.01 years was used and the integrator was run for a simulated time of 2000 years. At each step the eccentricity vector of the planet was calculated with:

$$\mathbf{e} = \left(\frac{v^2}{GM_\star} - \frac{1}{r} \right) \mathbf{r} - \frac{\mathbf{r} \cdot \mathbf{v}}{\mu} \mathbf{v} \tag{11}$$

The magnitude of the eccentricity vector is shown in Figure (4) with the plot of the analytical results using the method above for the same initial conditions overlaid. Different simulations were run with the same initial eccentricities as those in the analytical examinations of the equations. The analytical and numerical results are overlaid on top of each other.

Ida et al examine these force equations and others from Papaloizou & Larwood 2000, Coleman & Nelson 2014, and Daisaka et al 2006. They recommend as the equations of motion to use in N-body code to represent the forces felt by a planet in a gas disc:

$$\frac{\mathrm{d}\mathbf{v}}{\mathrm{d}t} = -\frac{v_K}{2t_a}\mathbf{e}_\theta - \frac{v_r}{t_e}\mathbf{e}_r - \frac{v_\theta - v_K}{t_e}\mathbf{e}_\theta \tag{12}$$

where $\mathbf{e}_r$ is the unit vector in the radial direction, and $\mathbf{e}_\theta$ is the unit vector in the azimuthal direction. To examine this formula with the Runge-Kutta integrator the elements of the velocity vector had to be separated into the radial velocity and azimuthal velocity at every time-step.

The angle θ the planet made as it orbited the star was used to get the unit vectors in the radial and azimuthal directions, with $\mathbf{e}_r = (\cos\theta, \sin\theta, 0)$ and $\mathbf{e}_a = (-\sin\theta, \cos\theta, 0)$. The radial velocity is $v_r = \mathbf{v} \cdot \mathbf{e}_r$, and the radial velocity vector is $\mathbf{v}_r = v_r \mathbf{e}_r$. The azimuthal velocity is $v_\theta = \mathbf{v} \cdot \mathbf{e}_\theta$, and the azimuthal velocity vector is $\mathbf{v}_\theta = v_\theta \mathbf{e}_\theta$. These unit vectors were calculated at every time-step and used to find the acceleration due to the planets interaction with the gas disc. This was added to the acceleration due to the gravitational influence of the sun. These numerical integrations were again carried out over a simulated time of 2000 years and overlaid with the corresponding results from the analytic examination of equation (6) are shown in Figure (5).

5 Genga

We used Genga [4], an open source N-body code designed specifically to run on GPUs. Genga takes advantage of parallelization on GPUs which allows faster computation of N-body interactions. The genga code has been modified to add in migration forces caused by planet-disc interaction. We added the possibility to use the Ida 2020 formalization with equation

(12), and added a flag to switch between that and the Cresswell & Nelson prescription from equation (10). Using Genga allowed for longer simulation time with more planets. We set up simulations with 100 bodies spread in a ring at 5 AU around a 1 solar mass star. The initial masses of the bodies were 10^{-1} Earth masses, or around 1 Mars mass. The initial eccentricities and inclinations were randomly allocated between 10^{-2} and 10^{-3}, (radians for the inclination).

6 Results

The final eccentricities, inclinations and masses of the bodies in one run after 10^6 years are shown if Figure (6). It shows the results for each of the prescriptions and for one run without damping. The difference between damping and no damping is quite clear, however each prescription produces equivalent results for both eccentricity and inclination. Semi-major axis damping is stronger for the Ida prescription. This is in agreement with Figure (1) which shows that t_a for the Ida prescription is shorter.

This setup was repeated five times, with different random realisations of the same initial conditions. The spread of eccentricity and inclination was varied slightly for each run resulting in different initial positions for all bodies. Density plots of the log of the orbital elements for each of these runs are shown in Figure (7). The distribution of semi-major axis is very similar within each of the prescriptions, with a slightly stronger semi-major axis damping for the Ida prescription. The distribution of eccentricity is very similar for both prescriptions. Almost all of the bodies end up with eccentricities lower than the dotted vertical line showing $e = H/r$. For the inclination there appears to be more random variation within each prescription, however there are no clear differences between the prescriptions. Figure (8) shows the combined distributions for each prescription along with the distribution resulting from no damping. It becomes clearer in this plot how similar both prescriptions are when compared to pure N-body simulations without damping. Without damping most of the final eccentricities of the planets are greater than $e = H/r$. About half of the final inclinations without damping are greater than $i = H/r$. The inclination damping here is stronger than the eccentricity damping. This can also be seen in Figure (6).

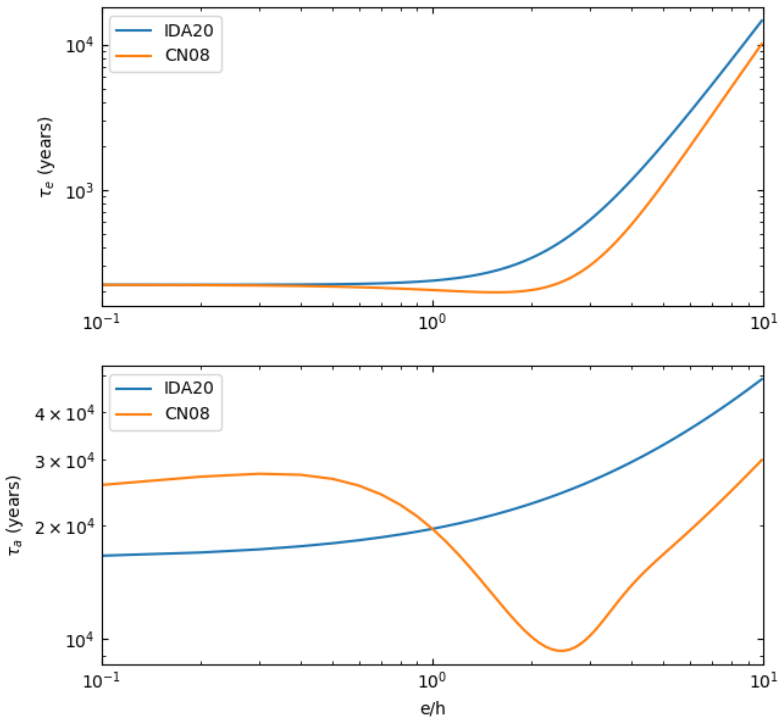

Figure 1: A comparison of the damping timescales using the prescriptions from Ida et al 2020 (blue curves) and Cresswell & Nelson 2008 (orange curves). The system here consists of a 10 Earth mass planet orbiting a 1 solar mass star at an initial semi-major axis of 1 AU. The first plot shows the eccentricity damping timescales. The damping timescale is shown in years plotted as a function of e/h where h is the scale height of the gas disc in terms of radial distance, with $h = 0.05$. Both prescriptions overlap for values of e/h of around less than 1, which corresponds in this case to eccentricities of less than 0.05, then as e/h increases t_e increases for both prescriptions, with that for Ida et at 2020 beginning the increase earlier. This indicates that at higher eccentricities the prescription from Ida et al 2020 predicts a longer circularization time compared to Cresswell & Nelson. The second plot shows the semi-major axis damping timescales. The x-axis is the same as in the first plot, with t_a in years on the y-axis. For the semi-major axis damping timescale the Cresswell & Nelson prescription shows a value of just under 2×10^4 years for an initial value of 0.1 for e/h, which then gradually increases as the initial eccentricity increases, until it reaches a value of 5×10^4 years for an initial value of e/h of 10. The Ida prescription has a different shape, beginning with longer semi-major axis damping timescales than the Cresswell & Nelson prescription, but then dips below it at higher values of e/h reaching a minimum at around $e/h = 2.5$ before rising again to values comparable to those for lower eccentricities. Overall the eccentricity damping timescale is strongly affected by initial eccentricity, increasing by two orders of magnitude at high eccentricities. However the semi-major axis timescale is only weakly affected by initial eccentricity. Both prescriptions give similar results for both timescales, with only small quantitative differences.

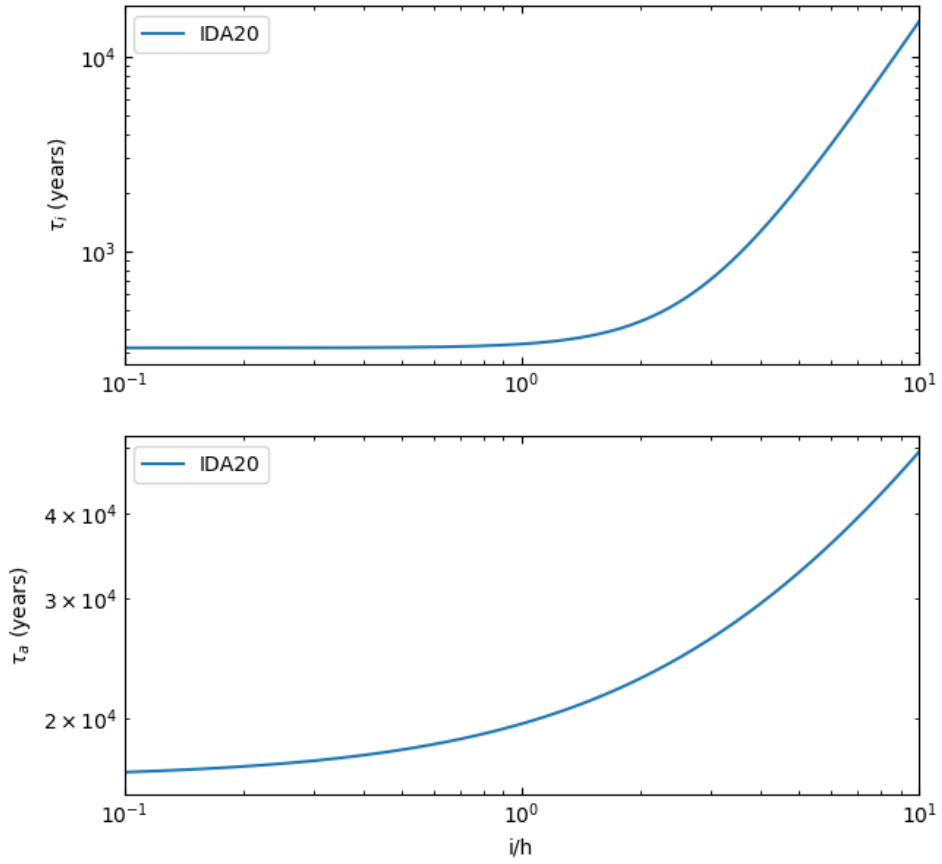

Figure 2: The inclination damping timescale, and the semi-major axis damping timescale using the prescriptions from Ida et al 2020. The values are for a 10 earth mass planet with an initial semi-major axis of 1 AU. The timescales are plotted as a function of i/h where h is the scale height of the gas disc in terms of radial distance, with $h = 0.05$. The planet has an initial eccentricity of zero in order to isolate the effect of initial inclination on the damping timescales. The inclination damping timescale is similar to the eccentricity damping timescale shown above, being relatively constant for low inclinations then increasing at initial values of i/h of greater than 1. The semi-major axis damping timescale is the same as it is when the initial inclination is zero and the initial eccentricity is non-zero, as shown above. This can be seen in equation (7), where setting either of e or i to zero and varying the other, will result in the same values for t_a.

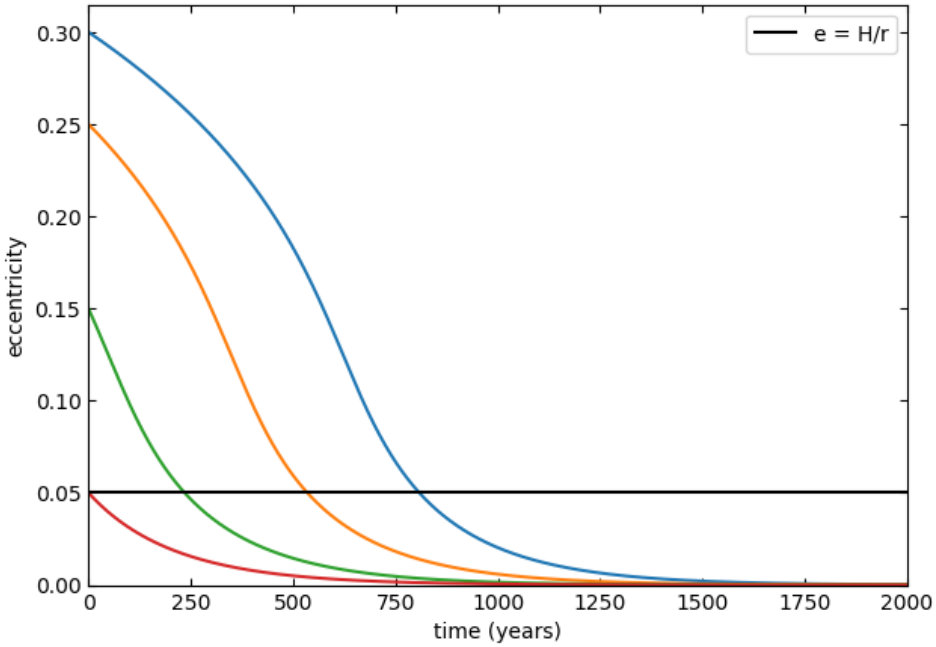

Figure 3: This shows the eccentricity evolution of a planet starting with several different initial eccentricities as predicted by Cresswell & Nelson 2008 from their prescription for eccentricity damping. The system is a 10 earth mass planet orbiting a 1 solar mass star at an initial semi-major axis of 1 AU with zero inclination. The plot was created by integrating using the Cresswell & Nelson 2008 eccentricity timescale formula and integrating it forward in time from an initial eccentricity. The solid horizontal line indicates where the eccentricity is equal to the scale height of the disc, where $e/h = 1$. This also seems to indicate a change in the shape of the curve of the change in eccentricity. When the eccentricity drops below this value the rate at which it continues to drop slows down. For each initial eccentricity the time in years on the x-axis when it drops to zero matches the corresponding eccentricity damping timescale in Figure (1). For low eccentricity ($e/h < 0.05$), the eccentricity damping timescale is independent of eccentricity as seen in Figure (1). We can see in equation 6 that at high eccentricity the damping timescale becomes proportional to e^3. The damping rate at high eccentricity is then $de/dt \approx e^{-2}$, while it is more efficient at low eccentricity.

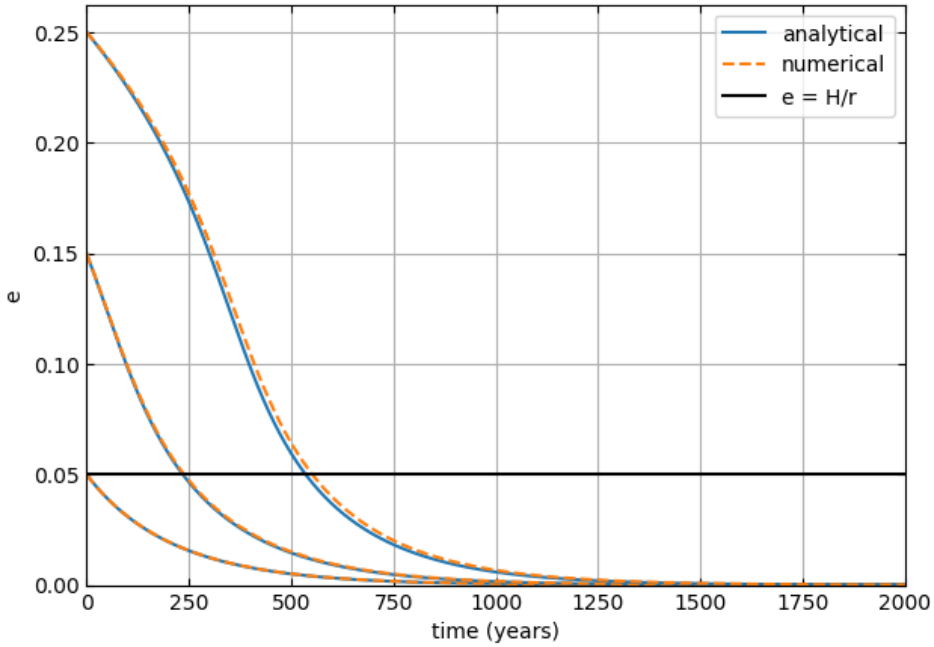

Figure 4: The eccentricity evolution of a planet orbiting a star calculated by two different approaches for each initial eccentricity as found using the prescription from Cresswell & Nelson 2008. The first is the same as in Figure (3), by integrating the eccentricity timescale equation, in this case equation (2), forward in time using Euler integration. This is shown in the plot as the blue pseudo-analytical line. The second approach is from numerical integration of the force equation, equation (10), using a 4th order Runge-Kutta integrator. At low initial eccentricities the two methods closely match each other, while at larger eccentricities there is a slight difference in the rate at which the eccentricity changes. This is likely a result of the inadequacies of the Runge-Kutta integrator. At higher eccentricities the planet will have a smaller perihelion. The closer the planet approaches the star the less accurate the integrator will be, as it uses a fixed time-step. Apart from this problem the results show that the two approaches are in agreement, with a time to circularization that matches the plots of the eccentricity damping timescales in Figure (1).

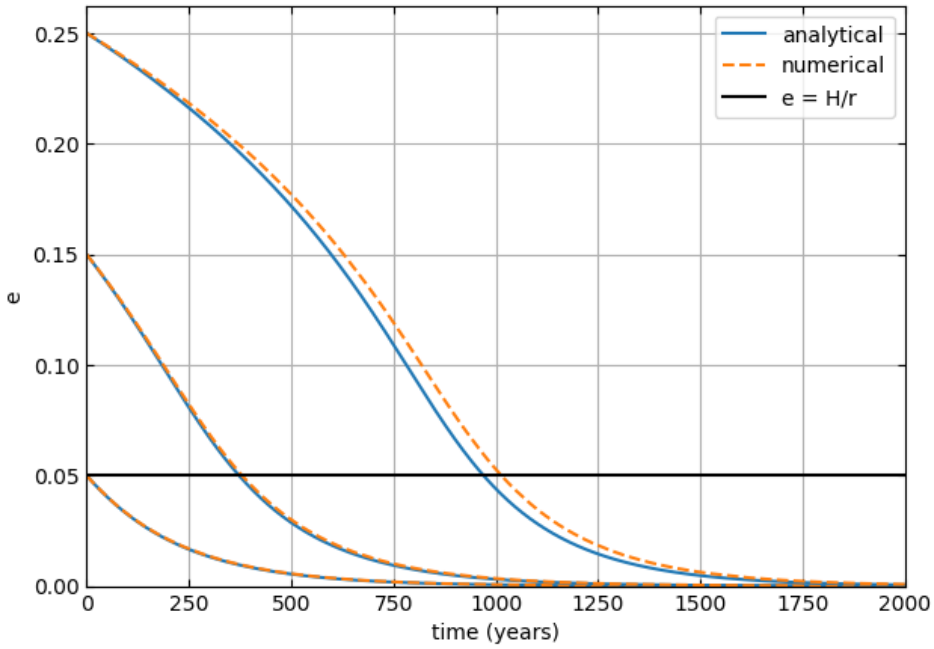

Figure 5: This shows the eccentricity evolution of the same planet orbiting the same star this time calculated using the prescriptions recommended by Ida et al 2020. The same three initial eccentricities were examined, and it can be seen that when compared to Figure (4) from the Cresswell & Nelson prescription, that the eccentricity damping happens at a slower rate. This agrees with Figure (1) showing that at initial eccentricities of around $e > 0.05$ the Ida prescription has a larger timescale than that of the Cresswell & Nelson prescription. The same problem as in Figure (4) with a slight difference in the results for the numerical and analytical approaches occurs here also.

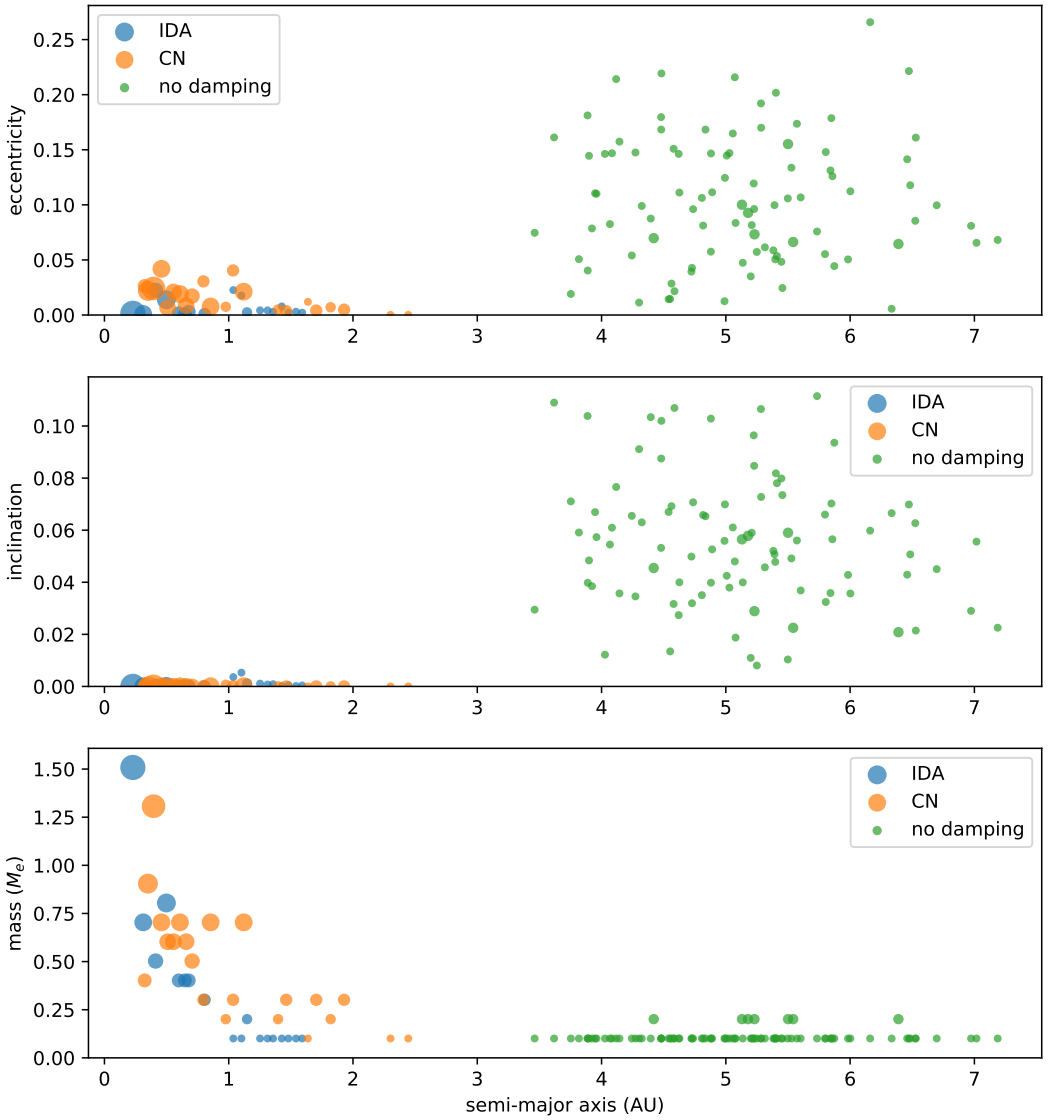

Figure 6: The three plots here show the distribution of eccentricity, inclination, and mass of bodies after 10^6 years. The mass is shown explicitly in the bottom plot, but is also indicated by the size of the markers for each planet. The diameter of the marker for each planet is proportional to the mass of the planet. The initial masses of all bodies was 10^{-1} Earth masses. There is stronger semi-major axis damping using the Ida prescription than the Cresswell & Nelson prescription. This can be seen in the larger amount of bodies at higher semi-major axis. Figure (1) shows why this should be the case. There we see that t_a for the Ida prescription is shorter than that for the Cresswell & Nelson prescription. Larger bodies are the result of collisions between two smaller bodies. In the simulation a collision creates a new body whose mass is the sum of the two smaller bodies. It is clear that more massive planets experience greater damping. Also shown are the results of a run with no damping. In this case there are also fewer collisions.

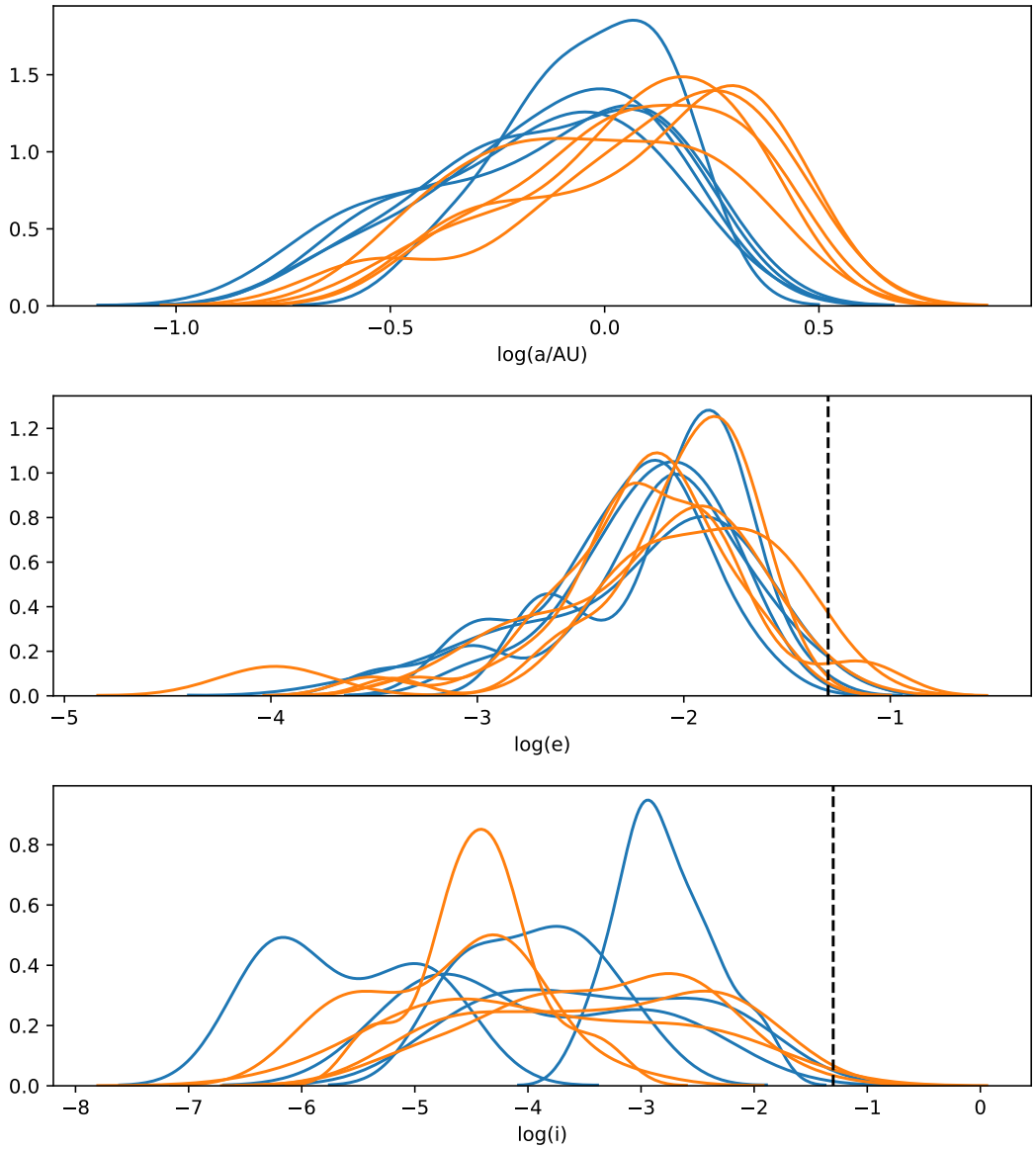

Figure 7: Density plots for the distributions of semi-major axis, eccentricity, and inclination for five different runs of the Ida prescription and five of the Cresswell & Nelson prescription. The simulations were run for 10^6 years. The logs of the values are shown on the x-axis. Also shown on is $e = H/r$ on the eccentricity plot and $i = H/r$ on the inclination plot. More semi-major axis damping can be seen for the Ida prescription. Each prescription produces similar final eccentricities. For inclination the results are not so clear. There is stronger inclination damping for both, so small random variations in inclination are easier to see.

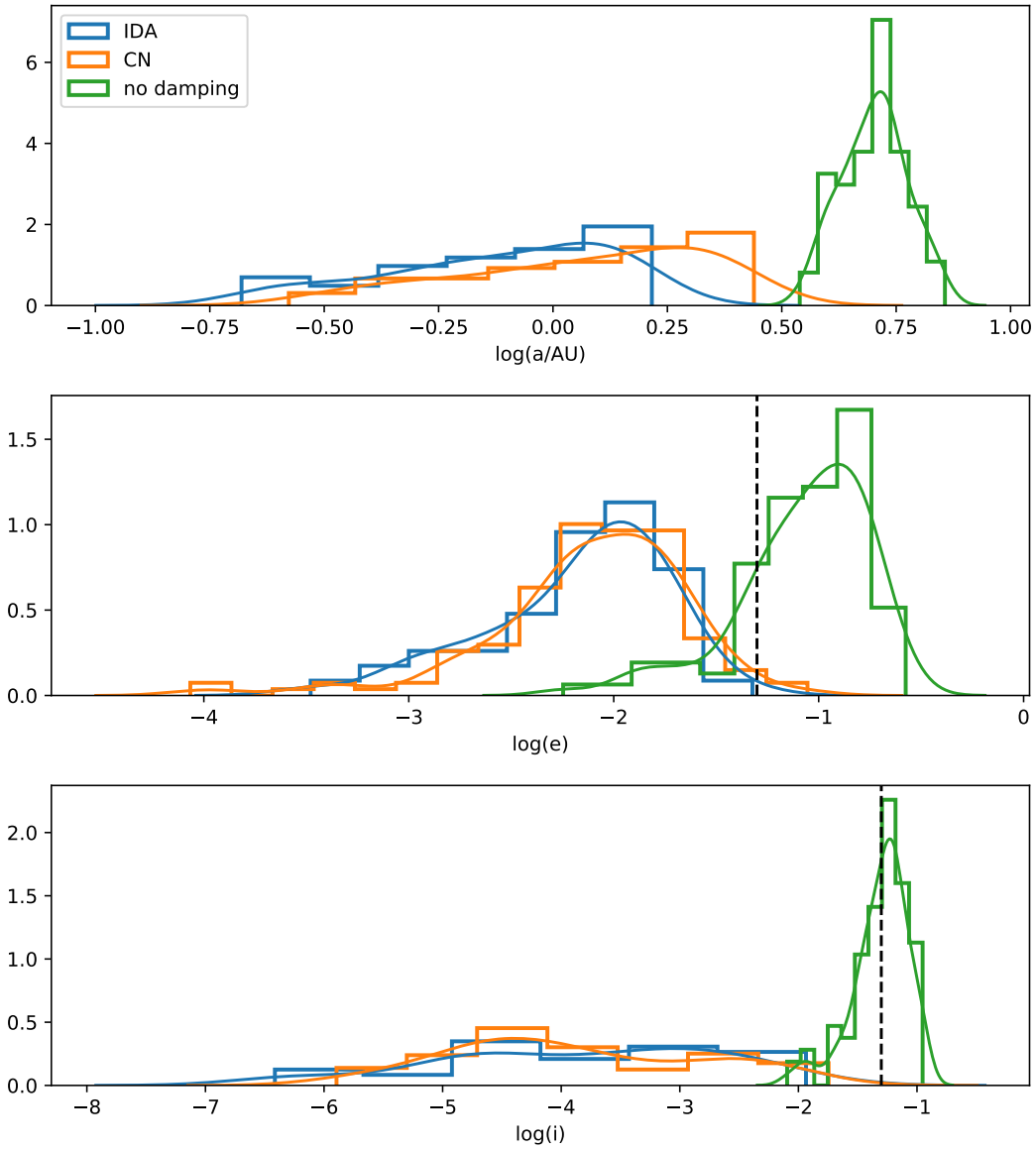

Figure 8: Histograms and density plots for the means of the distributions of semi-major axis, eccentricity, and inclination for five different runs of the Ida prescription and five of the Cresswell & Nelson prescription. The distribution of results for a run without any damping is also shown for comparison. Without damping the results are quite different. More semi-major axis damping can be seen for the Ida prescription but overall the results for each prescription are very similar to each other.

References

[1] S. Ida, T. Muto, S. Matsumura, and R. Brasser, "A new and simple prescription for planet orbital migration and eccentricity damping by planet-disc interactions based on dynamical friction," , vol. 494, pp. 5666–5674, May 2020.

[2] P. Cresswell and R. P. Nelson, "Three-dimensional simulations of multiple protoplanets embedded in a protostellar disc," , vol. 482, pp. 677–690, May 2008.

[3] H. Tanaka and W. R. Ward, "Three-dimensional Interaction between a Planet and an Isothermal Gaseous Disk. II. Eccentricity Waves and Bending Waves," , vol. 602, pp. 388–395, Feb. 2004.

[4] S. L. Grimm and J. G. Stadel, "The GENGA Code: Gravitational Encounters in N-body Simulations with GPU Acceleration," , vol. 796, p. 23, Nov. 2014.